Optimization of the parallel and mild hybrid vehicle platforms operating under conventional and advanced combustion modes

Jesús Benajes, Antonio García, Javier Monsalve-Serrano* and Santiago Martínez-Boggio

CMT - Motores Térmicos, Universitat Politècnica de València, Camino de Vera s/n, 46022 Valencia, Spain

Energy Conversion and Management
Volume 190, 15 June 2019, Pages 73-90

Corresponding author (*):
Dr. Javier Monsalve-Serrano (jamonse1@mot.upv.es)
Phone: +34 963876559
Fax: +34 963876559

Abstract

The stringent regulations, increased global temperature and customer demand for high fuel economy have led to rapid developments of different alternative propulsion solutions in the last decade, with special attention to the electrified vehicles. The combination of electric machines with conventional powertrains allows to diversify the powertrain architectures. In addition, alternative combustion modes as reactivity controlled compression ignition (RCCI) have been shown to provide simultaneous ultra-low NOx and soot emissions with similar or better thermal efficiency than conventional diesel combustion (CDC). Therefore, the combination of both technologies creates a promising horizon to be implemented in commercial vehicles of the near future. In this work, experimental and numerical simulations were combined to study the potential of the parallel full hybrid electric vehicle (P2-FHEV) and mild hybrid vehicle (MHEV) to obtain lower fuel consumption and NOx emissions than a conventional powertrain in the Worldwide Harmonized Light Vehicles Cycle (WLTC). The hybrid vehicles are simulated with both CDC and diesel-gasoline RCCI combustion engines as power source. Each powertrain was optimized in terms of components (battery, electric motors...) capacity, internal combustion engine operative points, energy management strategy and gear ratios. The results show a significant fuel consumption reduction as the complexity of the hybrid system increases. The parallel architecture, which represents the most complex hybrid system tested in this work, allows obtaining a fuel consumption reduction of around 20% as compared to CDC. The dual-mode CDC-RCCI concept showed improvements in NOx and soot emissions with comparable values in terms of energy consumption and CO_2 emissions than CDC. Additionally, the mild hybrid technology with the functionality of start-stop, torque assist and regenerative braking showed an acceptable balance between complexity and fuel consumption gain.

Keywords

Low temperature combustion; Mild hybrid vehicle; Full hybrid vehicle; Dual-fuel combustion; Driving cycles

1. Introduction

Due to growing concern about climate change, many car manufacturers and research groups have recently embarked on the development of "green cars," such as hybrid electric vehicles (HEVs) and electric vehicles (EVs) [1]. The hybrid-vehicle technology has made remarkable progress, and the number of hybrid electric passenger cars owned has drastically increased since 2010 [2]. However, there is a continuous effort to promote better fuel economy and lower emissions of these vehicles to make them more competitive. An important factor to consider is the high additional cost that is introduced in the aftertreatment system of the internal combustion engines (ICE) as well as what the hybrid propulsion system would entail. Their effective potential in real world driving conditions strongly depends on the performance of their Energy Management System (EMS) and on its capability to maximize the efficiency of the powertrain in real life as well as during Type Approval tests as the WLTC driving cycle [3].

Powertrain architecture, which refers to topological relation and energy flow among powertrain components, is a crucial index of HEV powertrain. Therefore, the design, selection and optimization of the architecture before the vehicle development is a critical procedure that depends on multiple factors. Therefore, identifying the best architecture and its required components in the development stage, is a very challenging task. The number of parameters increases with respect to the traditional powertrains due to the addition of electric motors, battery package and control systems, apart from the conventional hardware (internal combustion engine, transmission, differential, etc). Furthermore, HEV powertrain architecture interacts with several energy management strategies, further complicating the selection of an appropriate architecture [4]. The main HEV types could be divided into three categories depending on the complexity of the powertrain and the connection between the ICE and the vehicle wheels: Mild (MHEV), Full (FHEV) and Plug-in (PHEV) electric vehicle [5]. MHEV and FHEV have the advantage of not requiring to re-charge the batteries externally as in PHEV. However, the main source of energy necessary to move the vehicle is provide by the ICE. Therefore, as in conventional powertrains, the improvement in terms of efficiency and pollutant emissions is crucial [6].

Mild hybrid electric can be found in several commercial vehicles due to the small changes and investment needed to modify the conventional vehicle. This hybrid technology incorporates a small electric motor to assist the ICE in start-stop, idle and high load conditions. Also, this small electric motor can operate as electrical generator and convert part of the braking energy into electric energy [7]. In addition, it does not need a high power energy storage due to the small power rating of the electric motor. A 48 V electrical system may be able to meet the requirements [8]. A step further in complexity are the FHEV with higher electric motor capacity as well as battery package, and more complex control system. FHEV could be classified into three different architectures depending on the connection between the ICE and the vehicle wheels: Series, Parallel and Series-Parallel [9]. The parallel hybrid drivetrain has features that allow both the ICE and electric motor to supply their mechanical power in parallel directly to the driven wheels [10]. The major advantages of the parallel configuration over the other systems are that the generator is not required, the traction motor is smaller and the control system has lower complexity [11]. Hence, the overall efficiency

can be higher and the total cost of the vehicle lower [2]. However, the mechanical efficiency in some conditions could be lower due to the electric motor is always connected when the ICE works [12]. The high amount of options and parameters evidences that advanced investigation needs to be performed. In this sense, purely experimental research may not be convenient from an economic perspective. On the other hand, the simulation has come as a possible solution for such problems as a flexible tool with close results to those obtained experimentally. Additionally, it allows to study of a wider range in terms of capacity and performance parameters [13]. Also, the numerical simulation gives the possibility to perform a global analysis of the vehicle behavior in several real conditions that will be hard to reach in an experimental test bench. In addition, it is strongly recommended to feed the main models with experimental data to improve the simulation results [14].

Among the necessity of reducing the fuel consumption, the nitrogen oxides (NO_x) and soot emissions limits imposed by the emissions regulations for ICE engines are becoming more and more restrictive over the years, which represents a major concern for researchers and manufacturers. One solution is adding complex aftertreatment systems that reduce the vehicle emissions before reaching the atmosphere [15]. However, this solution implies adding expensive elements, which increase the total weight of the vehicle [16]. Alternatively, advanced combustion modes come as a potential solution of these points [17]. For example, the premixed low temperature combustion (LTC) strategies are being extensively studied nowadays as a way to reduce both pollutants directly during the combustion process [18]. The reactivity controlled compression ignition (RCCI) combustion, has been demonstrated to be more promising than previous LTC strategies such us the homogeneous charge compression ignition (HCCI) [19] and diesel partially premixed combustion (PPC) [20]. This is mainly because RCCI is able to achieve thermal efficiencies near 50% in a wide range of engine speeds and loads, with engine-out NO_x emissions under the Euro 6 limits and simultaneous ultra-low soot emissions [21,22]. Despite the advantages of this combustion mode, there are several problems such as high amounts of unburned HC and CO emissions [23]. Additionally, using high proportions of low reactivity fuel (gasoline, ethanol,…) at high loads results in problems of excessive peak pressures and pressure rise rates in the combustion chamber [21]. Therefore, the implementation of the LTC technology, as the RCCI mode, is still restricted to moderate loads. Some approaches have been investigated to overcome these problems. One interesting solution is to use the conventional diesel combustion (CDC) mode in the points that cannot be reached with RCCI. Therefore, this solution requires low level of geometric and hardware modifications.

Electrification combined with advanced combustion modes seems to have potential in order to reduce the total CO_2 emitted by the vehicle fleets [24]. For this purpose, the use of an advanced combustion mode in a conventional, mild and full hybrid electric vehicle is studied in this work. The main goal is to evaluate the benefits of coupling a hybrid vehicle architecture with an ICE operating under CDC and CDC-RCCI mode. The second objective of this work is to define a methodology to optimize hybrid powertrains based in an already developed ICE. Experimental steady-state maps from fuel consumption and emissions were measured in a test bench for a high CR light-duty diesel engine (17.1:1). The engine maps were used as boundary conditions to estimate the

transient performance of the different vehicles. Therefore, three vehicle models were developed and optimized in GT-Suite 2018 (v2018, Gamma Technologies, LLC., Westmont, IL, USA, 2018) to evaluate the conventional, mild and parallel hybrid powertrains. Values of fuel consumption as well as emissions were assessed by the legislation used for homologation purposes in Europe, worldwide harmonized light vehicles test procedure (WLTP) [25]. This allows the analysis of the impact of different driving cycles and operating conditions on CO_2 emissions, energy management strategies, parameters selection, and the hybrid architectures. In addition, the total emission of CO_2 for each case is presented and discussed to investigate the potential of the hybrid concept to meet the future CO_2 targets.

2. Materials and methods

2.1. Engine, fuels and test cell

For the simulation of the driving cycles in various powertrain technologies it is necessary to obtain the engine maps of the two combustion modes that will be studied (CDC and dual-mode CDC-RCCI). Thus, experimental tests were carried out on an active dynamometer using the Euro 4 GM 1.9L light-duty engine in single-cylinder engine configuration and without including any aftertreatment system. This allows greater control of the input and output variables of the ICE, mainly during the engine calibration under dual-mode diesel-gasoline combustion. After that, the results were scaled to a 4-cylinder engine, which is the engine configuration that will be used in the vehicle simulation. The cylinder head is composed of four valves (2 intake-2 exhaust) operated by double cams, and the piston used is the serial one provided by GM. The compression ratio is set at 17.1:1 and the swirl ratio was fixed at 1.4 by using tangential and helical valves located at the intake port. Table 1 summarizes the most relevant characteristics of the engine.

Table 1. Main ICE characteristics.

Engine Type	4 stroke, 4 valves, direct injection
Number of cylinders	1
Displaced volume	477 cm^3
Stroke	90.4 mm
Bore	82 mm
Piston bowl geometry	Re-entrant
Compression ratio	17.1:1
Rated power @ 4000 rpm	27.5 kW
Rated torque@ 2000-2750 rpm	80 Nm

The injection system was adapted to operate with two fuels (diesel and gasoline), as depicted in Figure 1. The diesel fuel EN590 was injected into the cylinder by means of a solenoid direct injector (DI) located in the center of the cylinder. The gasoline fuel was injected into the intake port by means of a port fuel injector (PFI). The injection settings were handled using a DRIVVEN and Genotec controller units, respectively. The mass flow of both fuels was measured using dedicated AVL 733S fuel balances (AVL LIST GmbH, Graz, Styria, Austria). The main characteristics of the direct and port fuel injectors are shown in Table 2, and the most relevant properties of the fuels are summarized in Table 3.

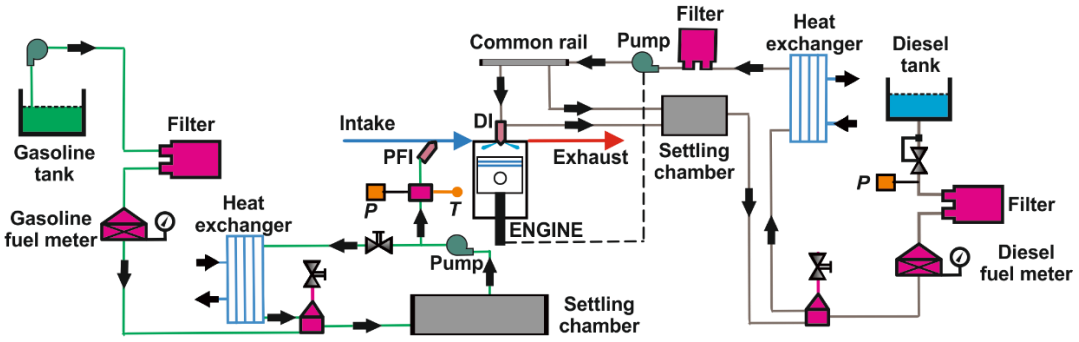

Figure 1. DI and PFI systems configuration.

Table 2. Main characteristics of the DI and PFI.

Direct injector		Port fuel injector	
Actuation Type [-]	Solenoid	Injector Style [-]	Saturated
Steady flow rate @ 100 bar [cm^3/min]	880	Steady flow rate @ 3 bar [cm^3/min]	980
Included spray angle [°]	148	Included Spray Angle [°]	30
Number of holes [-]	7	Injection Strategy [-]	single
Hole diameter [µm]	141	Start of Injection [CAD ATDC]	340
Maximum injection pressure [bar]	1600	Maximum injection pressure [bar]	5.5

Table 3.Main physical and chemical properties of the fuels.

	Diesel EN590	Gasoline EN 228
Density [kg/m^3] (T= 15 °C)	842	747
Viscosity [mm^2/s] (T= 40 °C)	2.929	0.545
RON [-]	-	197.6
MON [-]	-	89.7
Cetane number [-]	51	-
Lower heating value [MJ/kg]	42.50	44.09

An active electric dynamometer is used to control the engine speed and load during the experiments. The test cell scheme in which the engine is operated can be seen in previous work [22]. The intake line is composed of a screw compressor, which supplies fresh air to the engine at high pressure as does the turbocharger in a multi-cylinder engine. Additionally, a heat exchanger, air dryer and other equipment as flow, pressure and temperature meters are added to control the conditions of the air at the engine intake. A settling chamber is included to reduce the fluctuation of the pulse in the intake duct. The exhaust gas recirculation (EGR) line is also introduced into the intake line, downward the settling chamber. The temperature of the EGR gases are monitored at several points along the line. Finally, the pressure and temperature of the air-EGR mixture are measured in the intake manifold before entering into the cylinder. On the other hand, the exhaust line is composed of similar elements than the intake line. The more relevant difference is the addition a pneumatic valve, which is use to reproduce

the backpressure caused by the turbocharger in the 4-cylinder commercial engine. Finally, there is the Horiba MEXA-7100 DEGR emission analyzer and an AVL 415S smoke meter.

The engine map was discretized in 80 different operation points with 20 of them falling inside the RCCI condition. Each stable state operating point is measured three times over a period of 60 seconds. An average of each stable point, plus the interpolation of the map with the proximity tool, is performed to obtain the engine calibration map in the range of 1000 – 4500 rpm.

2.2. Single-cylinder engine maps

The experimental maps obtained from the test bench are presented in Figure 2 and Figure 3 for pure diesel and dual-mode CDC-RCCI. Engine maps for CO, HC, soot and CO_2 are presented in the appendix for brevity of the manuscript. The area falling within the dashed line corresponds to that in which the engine operates under RCCI operation. In the rest of the map, the engine runs under conventional diesel combustion. The gasoline percentage used in each point of the map, calculated as the ratio between the gasoline mass and the total injected mass, can be seen in Figure 4. As can be inferred from the maps, the RCCI operation allows a notable reduction of NO_x and soot compared to the surrounding diesel operation area. By contrast, CO and HC emissions are notably increased. In terms of fuel consumption and CO_2 emissions, the figure shows that the dual-fuel portion slightly penalizes the global map. Figure 4 shows that the gasoline fraction used in the RCCI portion of the map ranges from 30% to 80%. The details of the engine calibration procedure can be found in [26].

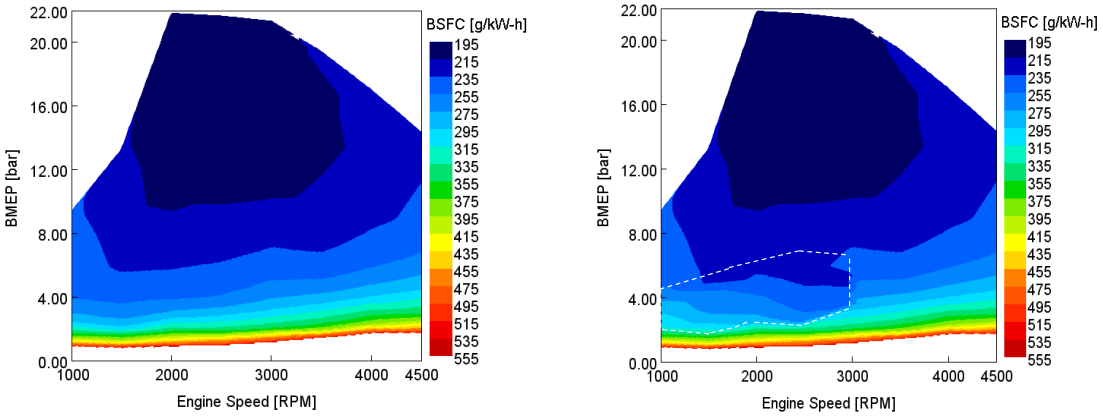

Figure 2. Fuel consumption (g/kWh) for pure diesel (a) and the dual-mode CDC-RCCI concept (b).

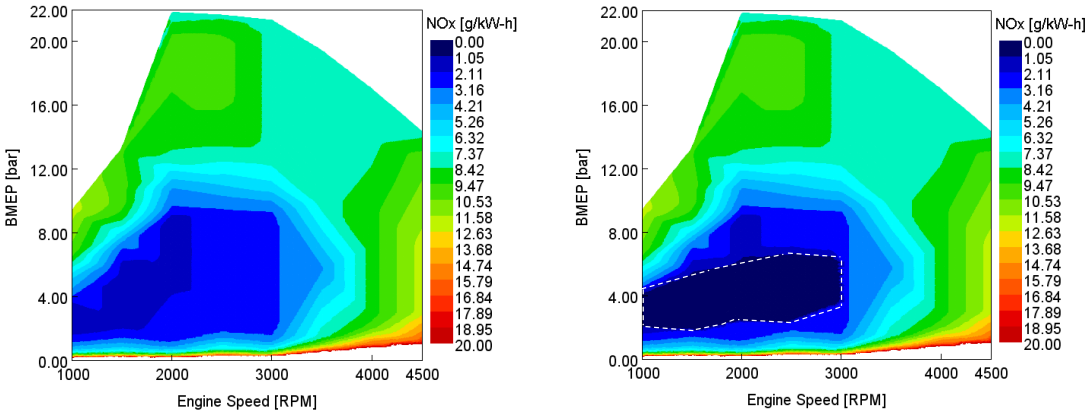

(a) (b)

Figure 3. NO_x Emissions (g/kWh) for pure diesel (a) and the dual-mode CDC-RCCI concept (b).

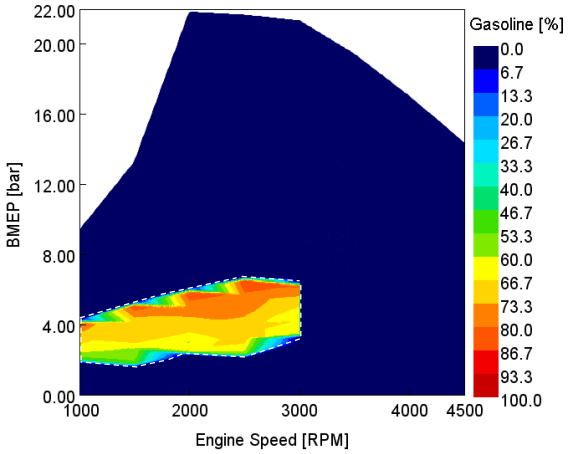

Figure 4. Gasoline fraction map for the dual-mode CDC-RCCI concept.

2.3. Vehicle, hybrid powertrain models, selection of components and driving cycles

2.3.1. Vehicles characteristics

The vehicle selected to perform the simulations is the Opel Vectra, which equips the compression ignition engine used in the experimental tests. The aerodynamic and mechanical characteristics of the original equipment manufacturer (OEM) vehicle are described in Table 4. This car is inside the large family car type, defined as a mid-size car in the North American and Australian standard, and D-segment in Europe. Also, it is a car segment that presents potential to hybridization due to having enough space to incorporate battery package and electric motors. In addition, the fuel consumption reduction in this type of vehicles is necessary due to their high power (over 120 HP) and weight (over 1500 kg) [27]. For this reason, several companies have already applied mild and full hybrid powertrains in this type of cars [28].

Table 4. Vehicle specifications.

Vehicle type [-]	OEM
Base vehicle Mass [kg]	1523
Passenger and Cargo Mass [kg]	100
Fuel Mass [kg]	45
Vehicle Drag Coefficient [-]	0.28
Frontal Area [m²]	2.04
Tires Size [mm/%/inch]	225/45/R118
Differential ratio [-]	3.2

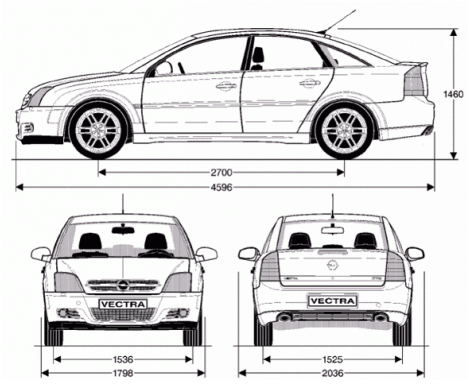

2.3.2. Mild and Parallel Hybrid powertrain models

The study of the different proposed powertrains was evaluated using the commercial software GT-Suite of Gamma Technologies® (v2018, Gamma Technologies, LLC., Westmont, IL, USA, 2018). The GT-Suite package allows the simulation of the entire vehicle. This involves models of gearbox, tires, axles and couplings, etc. In addition, the software also has the necessary devices to perform the hybridization process, as different electric motors (EM), batteries and controllers. Moreover, the software allows the incorporation of driving cycles with their respective load, acceleration profile, and performance in different environmental conditions. In this way, the experimental engine maps were used as inputs for the simulation.

The dynamic simulation model consists of a driver sub-model trying to follow a predetermined speed profile. The desired torque is calculated by the vehicle traction equations taking into account the road friction and aerodynamic forces, among others [22]. In particular, the driver module represents the driver actions that control the accelerator pedal, brake pedal, and transmission gear number during driveway and shifting. Therefore, the model consists of a feed forward component which calculates the ICE+EM load torque required to achieve the desired vehicle speed. Additional sub-models are the environment model, used to specify the ambient air conditions (that affect the aerodynamic forces on the vehicle), and the road module, that contains the road properties (that affect the vehicle dynamics). Moreover, a braking module is introduced to calculate the brake pedal position based on the desired braking power and maximum torque capability of the brakes.

For this study, three different models were proposed to be simulated, including MHEV, parallel FHEV and the conventional powertrain for comparison (baseline case). The baseline case was modeled as an ICE, the transmission coupled with the engine through a clutch and also connected to the differential that propel the wheels. Moreover, the model incorporates a sub-model of the brakes, tires and axles behavior apart from other couplings present in the powertrain. More information of the conventional powertrain can be found in a previous work of the research group [22]. Unlike conventional powertrain, the HEV architecture requires the use of more elements. The main differences with respect to the conventional powertrain are the number of controllers and the addition of more components as battery package and electric motor, which are used to propel the wheels, recover energy or as range

extender. In addition, each specific architecture can propel the vehicle in different modes by changing the states of the coupling devices. Basically, it can be defined three states: a) only the EM (pure electric mode), b) only the ICE (conventional powertrain) and c) combined EM-ICE (dual propulsion mode). Since the FHEVs cannot charge the batteries with external agents (contrarily to the PHEVs), during the simulations it was imposed that the state of charge (SOC) at the end of the driving cycle must be equal or greater than the initial one ($SOC_{end} \geq SOC_{ini}$). This allows to perform a fair comparison of the energy consumption between the different concepts.

Other fundamental element in hybrid powertrains is the control system, which defines which state that will be used in each operating condition of the driving cycle. It can be divided into two levels. The high level (or main control), manages all the signals of the vehicle. It is also called Supervisor, and it controls and gives commands to low level controllers (local or component controllers). The low-level control units include the engine controller (ECU), the transmission controller (TCU), the battery management system (BMS) and the brake controller, among others. Moreover, the system is fed back internally with information (main signals of the components) to change the powertrain state according to the primary programming. A vast range of supervisory controller systems have been proposed in the past, ranging from rule-based control (RBC) to optimization based control strategies (dynamic, static, real-time optimization) [29]. The advanced controllers are seen to hold high potential, but the impact so far has been mainly within academic circles. Therefore, the heuristic strategies (as RBC) are still more prevalent due to their simplicity and effectiveness in commercial cars [30]. For this reason, and because the focus of this work is to see the potential of RCCI combustion in already stablished hybrid technologies, the power manager strategy that was used is the RBC. A narrow band was used to charge the battery with a threshold value of 0.58 (called as SOC_{charge}). Therefore, the ICE starts to charge the battery when the SOC is below SOC_{charge} and finishes when the system reaches the SOC_{target}, that for this work is the initial one (SOC_{ini}).

Figure 5 and Figure 6 show a scheme of both models used to simulate the MHEV and FHEV-P2 powertrain. Basically, both systems are composed of the conventional systems included in the baseline case, with the addition of an electric motor, battery package and new controllers for the extra components. As was described in the previous section, the supervisory controller has the function of managing the operating mode using as inputs the signals from the different hardware and other control units. For these two hybrid powertrains, the supervisory RBC code was programed to provide the follow functions: power-assist, regenerative braking, start-stop and battery charging modes. Other control units that are common for both models are the BMS, which calculates the power available in the system and the maximum discharge and charge rates; the ECU, which sets the accelerator position, ICE limits and idle condition; and the TCU, which sets the gear position depending on the vehicle speed and gear strategy.

The main difference between the MHEV and FHEV-P2 is the position and capacity of the electric motor. In the case of the mild hybrid, the system substitutes the conventional starter and alternator by a unique electric motor with higher power and

efficiency. It is also called Belted Alternator Starter (BAS) because it is located in the serpentine belt (old alternator position). This solution minimizes the changes needed in the already developed engines, and for this reason several companies include them in their standard vehicle architectures. However, the electric motor cannot move the vehicle by itself due to the low capacity and the coupling system. For this reason this solution is considered as a first step between conventional and complex hybrid vehicles [31].

On the other hand, the parallel hybrid powertrain is a FHEV due to the capacity of the electric motor, which has the capability to propel the vehicle at low, medium and high vehicle speeds [32]. This powertrain basically works with an ICE and EM connected with a clutch to provide driving torque to the wheels, separately or together [28]. Often named as pre-transmission parallel hybrid (P2-FHEV) due to the ICE and EM torques are modified by the transmission, as can be seen in Figure 6. Therefore, the ICE and EM must have the same speed range. Moreover, as shows Figure 6, other elements present in this powertrain are the transmission, two clutches and the battery package. The RBC for the FHEV-P2 includes all the capabilities described in the MHEV, with an additional operation mode in which the EM propels the vehicle depending on the SOC level and the vehicle speed.

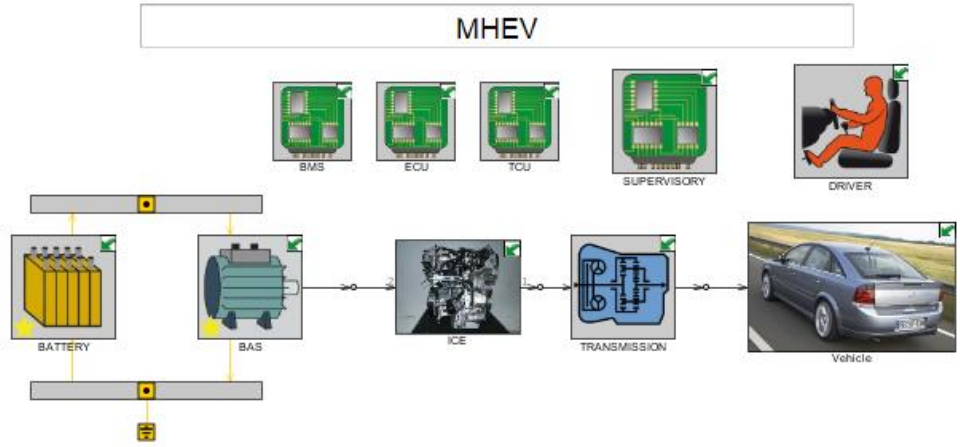

Figure 5. Mild Hybrid vehicle model developed in GT- Power® for the Opel Vectra.

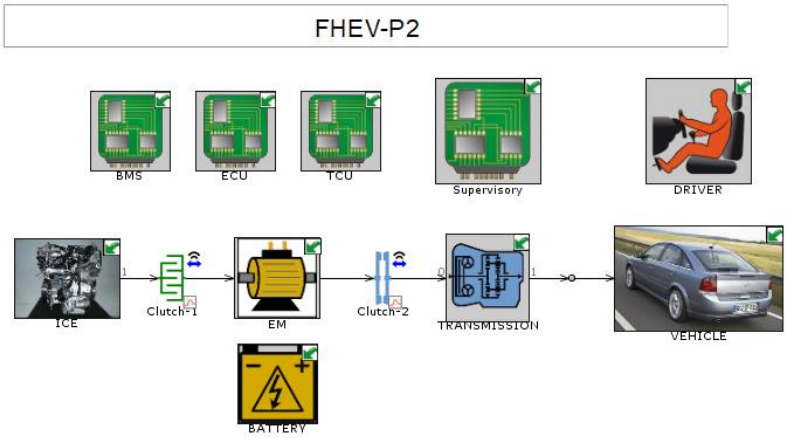

Figure 6. Parallel Hybrid vehicle model developed in GT- Power® for the Opel Vectra.

A summary of the operation modes defined in the supervisory control unit is detailed in Table 5. As was mentioned before, the main difference of FHEVs with respect to MHEVs is the possibility to impulse the vehicle in pure electric mode (clutch 1 disengaged at Figure 6). As vehicle speed increase ($V > V_{limit}$) or battery SOC drops below pre-defined threshold value (SOC_{charge}), the supervisory pass to HEV mode and the ICE will be ignited and clutch engaged gradually. During the transition mode, the EM may play the roles of traction motor and starter (ICE start). The speed limit is imposed as parameter to be optimized with the limits between 25 and 140 km/h.

If the vehicle speed is zero ($V = 0$), three states can be possible: 1) ICE off and driver pedal position at 100%, 2) ICE off and EM motor providing torque to start the ICE ($Start_T$) and 3) Battery charging with the ICE at idle speed. The selection of these two modes depends on the SOC level and the ICE speed.

When the vehicle is moving ($V > 0$) and accelerating ($Driver_T > 0$) four states are possible: 1) Engine Starting and the EM motor giving the power to move the vehicle up to the ICE rotational speed increase, 2) Power assist (PA) mode in which the driven torque is divided between the ICE and the EM (50-50%), 3) ICE-alone traction mode in which the electric motor is de-energized and the vehicle is propelled only by the ICE. This mode is used when the SOC of the batteries is in the high region ($SOC > SOC_{target}$), and the EM motor cannot give the require power in the PA mode and 4) Charging mode in which the ICE provides the torque to drive the vehicle and charge the battery package due to $Charge_{State} = 1$ (it is at 1 when $SOC < SOC_{charge}$ and changes to 0 when $SOC > SOC_{Target}$). Thus, the electric motor operates as a generator. Finally, there is an additional sub-state, Power Assist Max ICE, in which the necessary torque is more than that the ICE can provide, so that the electric motor assists the ICE. This last mode gives to the hybrid vehicle an extra power with respect to the conventional powertrain.

The last vehicle state is when the vehicle is braking ($Driver_T < 0$) but the $V > 0$. Three states are possible depending on the SOC and the capability of the EM to recovery the energy: 1) Regenerative braking mode, the engine is shut down and the electric motor is operated to produce a braking torque to the drive the train. Part of the kinetic energy of the vehicle mass is converted into electric energy and stored in the batteries, 2) Braking mixed, both the electric motor and the conventional friction brakes deliver traction power to decrease the vehicle speed due to the EM motor is not capable to stop the vehicle and 3) Conventional breaking, in which the friction brakes deliver the necessary toque to decrease the speed of the car because it is not necessary energy recovery ($SOC > SOC_{max}$). See Table 6 for more details of the condition necessary of each state.

The charge torque ($Charge_T$) was set to be calculated by a PID system depending on the difference between the actual SOC and the SOC_{target}. For all the hybrid models was set a proportional gain to impose the maximum generator power when SOC = 0.40. This allows the system to not reaching the minimum admissible SOC value of 0.30 in any condition if the electric motor is well dimensioned. Therefore, for intermediate values of SOC (between 0.64 and 0.40) the charge torque is proportional to the demand SOC.

Table 5 .Operation mode of Supervisory Controller for HEV and FHEV-P2.

Vehicle State	Sub-state	ICE State	ICE Req	EM Req
Electric Vehicle mode (EV)*	Zero	Off	0	0
	EV	Off	0	$Driver_T$
Hybrid Electric vehicle mode (HEV) - Vehicle Stop	Zero	Off	0	0
	ICE Start	Off	0	$-Start_T$
	Idle Charging	On	$Charge_T$	$-Charge_T$
Hybrid Electric vehicle mode (HEV) - Vehicle Moving and Accelerate	ICE Start	Off	0	$Driver_T + Start_T$
	Power Assist	On	$0.5 * Driver_T$	$0.5 * Driver_T$
	Normal	On	$Driver_T$	0
	Power Assist Max ICE	On	ICE_{maxT}	$Driver_T - ICE_{maxT}$
	Charging	On	$Driver_T + Charge_T$	$-Charge_T$
Hybrid Electric vehicle mode (HEV) - Vehicle Moving and Braking	Regenerative Braking	Off	0	$Driver_T$
	Breaking Mixed	Off	0	$EMmin_T$
	Breaking	Off	0	0

*Only for FHEV-P2 due to the position and capacity of the EM.

Table 6 .Conditions for each operation mode of Parallel Hybrid Vehicle.

Vehicle State	Sub-state	Conditions	
EV	Zero	$V = 0$	$Brake_{Position} = 100\%$
	EV	$0 < V < V_{Limit}$	$Charge_{State} = 0$
HEV - Vehicle Stop	ICE Start	$V = 0$	$Charge_{State} = 1$ & $ICE_{Speed} < 1000$ rpm
	Idle Charging		$Charge_{State} = 1$ & $ICE_{Speed} > 1000$ rpm
HEV - Vehicle Moving and Accelerate	ICE Start	$Driver_T > 0$ & $0 > V > V_{Limit}$	$ICE_{Speed} < 1000$ rpm
	Charging		$Charge_{State} = 1$
	Power Assist		$Charge_{State} = 0$ & $0.5 * Driver_T < EM_{maxT}$
	Power Assist Max ICE		$Driver_T > ICE_{maxT}$ & $SOC > SOC_{min}$
HEV- Vehicle Moving and Braking	Regenerative Braking	$Driver_T < 0$ & $V > 0$	$SOC < SOC_{max}$ & $Driver_T < EM_{MinT}$
	Breaking Mixed		$SOC < SOC_{max}$ & $Driver_T > EM_{MinT}$
	Breaking		$SOC \geq SOC_{max}$

2.3.3. Selection of components

As the main goal of this work is to optimize each powertrain to perform a homologation driving cycle with the lowest fuel consumption and NO_x emission, it is necessary to select properly the size and capacity of the components for each powertrain. For this reason, it was used an optimization methodology for HEV previously developed by the authors and used in series hybrid architecture [33]. First, the limits in terms of size, capacity and weight to be considered in the design of experiments (DoE) for each component and powertrain are studied. Then, the Latin hypercube DoE method was used to determine the relationships between the independent (factor) and dependent (response) variables. The advantage of this method is that it requires lower number of cases to perform the study than the traditional full factorial method. This reduces the computational cost as well as the time needed to complete the study. On the other hand, due to the distribution of the cases, a detailed study of the whole range

of the proposed operating conditions is possible. In this work, 800 cases were selected for each powertrain and combustion mode. Therefore, a total amount of 3200 different set ups were analyzed. From the results of the DoE, different response models are adjusted using the Kriging adjustment method increasing the number of cases studied without the need to launch the case [34]. The precision of the model was evaluated by the R^2 values and the graphic dispersion of the observed and predicted values. For the two engine maps and powertrain configurations, the precision was over 92%. As the main requirement for this study was to achieve low consumption and NOx emissions, the optimum cases were selected in a balance of these two parameters. Finally, the adjusted models are used to determine the Pareto frontier defined as the minimum fuel consumption and NO_X.

The emissions regulations are very restrictive about the pollutant levels from passenger vehicles [35]. To achieve the current standards, complex aftertreatment systems have been developed. Among the different devices that are incorporated to the vehicle, the selective catalytic reduction (SCR) is the responsible of reducing the NO_x emissions in diesel engines. Basically, this system converts the engine-out NO_x into diatomic nitrogen (N_2) and water (H_2O). To improve this reaction, anhydrous ammonia (also called Urea), is injected into the system. Therefore, the use of the SCR adds an extra fluid consumption to the vehicle. To obtain the urea consumption in the WLTC cycle, the method proposed by Johnson [36] was used. Thus, considering the engine-out emissions (NO_x) and the Euro 6 limit for this pollutant ($NO_{xEU6} = 0.08$ g/km) the Urea mass ($\dot{m}_{urea}$) per kilometer in the SCR system was estimated by means of Eq.1. Later, the urea mass was added to the fuel mass consumption ($\dot{m}_{fuel}$) to obtain the total fluid mass consumption ($\dot{m}_{Total\ mass\ cons}$) shown in Eq. 2. This parameter was selected to be minimized during the optimization process because this approach allows to include both fuel and NOx (indirectly) in a single variable.

$$\dot{m}_{urea} = \frac{(NO_x - NO_{xEU6}) * 0.01 * m_{fuel}}{Travel\ Distance}\ \text{[g/km]} \quad (1)$$

$$\dot{m}_{Total\ mass\ cons} = \dot{m}_{urea} + \dot{m}_{fuel}\ \text{[g/km]} \quad (2)$$

In the optimization process, it is necessary to test several operative conditions and components set ups like capacity and weight, among others. The main components added in the hybrid powertrain are the EM and battery package. The function of the EM is to transfer the electric energy to the mechanical one (traction motor) or the other way around (generator motor). Both, HEV and FHEV-P2, use the same EM for both functions. In this way, the conversion efficiency is the main parameter needed to be modeled for each operative condition requested. Generally, electric motors for HEV needs durability and high efficiency to operate with frequent starts and stops, high rates of acceleration and deceleration, high torque and low-speed (hill climbing events), low torque and high-speed (cruising events), and a very wide speed range of operation (0-9000 rpm). Among all passenger EVs and HEVs, a very small number of companies use induction motors (IM) or surface mount permanent magnet (SPM) machines. Almost all the other major car companies use interior permanent magnet (IPM) machines due to their high torque

density and efficiency. Therefore, the IPM type with the same efficiency map (Figure 7) was used for both HEV architectures to have comparable platforms.

The efficiency map against engine speed and torque shown in Figure 7 corresponds to a commercial EM available in the literature [37] (developed by Toyota Motor corporation and applied in the Prius 2016 among other hybrid vehicles). In this work, the efficiency map was adapted to operate with better efficiency at the typical diesel ICE speed (around 2000 rpm) instead of the typical speed in gasoline ICE (3000 rpm). In addition, the maximum torque was changed to cover a wide range of possible electric motors design in the optimization process. For the MHEV, some studies suggest that EM of power typically 7–12 kW is enough for this type of technology [38]. Others authors affirm that the power rating of the electric motor may be in the range of about 10% of the engine power (equivalent to 10.5 kW for the Opel Vectra) [39,40]. Therefore, a range around the suggested value was tested in this work (from 3 to 25 kW). On the other hand, the literature review does not bring an optimum value of electric motor capacity in the case of parallel hybrid vehicles, and has a great variation depending on the vehicle and the driving cycle tested. In the market, it can be found vehicles having EM of 15 kW as the Honda Insight, as well as with 90kW as the Mercedes-Benz E350. However, in this last case the ICE is rated at 250 kW. Therefore, a medium-term range was adopted in this simulation campaign. The maximum power and average weight/power for each EM in the different HEV configuration is shown in Table 7.

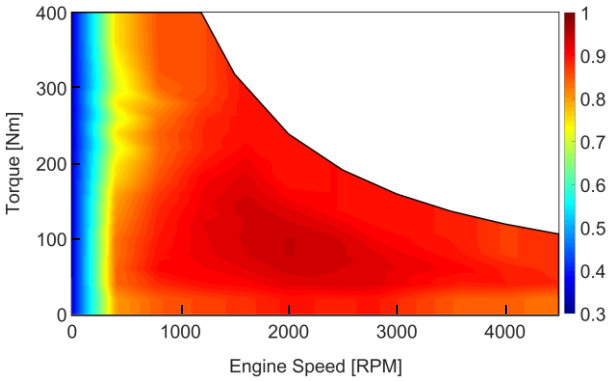

Figure 7. Efficiency map of the Electric Motor.

The other main component of the HEV is the battery package. The two main battery types that have been implemented in EVs and HEVs are of the Nickel-Metal-Hydride (NiMH) and the Lithium Ion (Li-Ion) family. The last one is better than NiMH batteries in terms of energy density, specific energy and specific power. In this work, Li-Ion battery was used and the behavior was simulated by Thevenin electrical-equivalent model [41], consisting of open-circuit voltage and internal resistances. Each parameter of the circuit are defined as a function of SOC and current through the terminals of the battery. Actually, not all the energy stored in the energy storage can be fully used to deliver sufficient power to the drive train. Low SOC (below 0.30) will limit the power output, and will lead to a low efficiency due to an increase of internal resistance. In addition, battery manufacturers recommend maximum SOC values around 0.70. For this reason, it was selected a medium initial SOC value (0.64) that is used to SOC_{target} at the end of the driving cycle and a band up to 0.58 to start the charge by the ICE. For the MHEV, the 48 V system instead of traditional 12V was preferred due to the potential of

the higher voltage to increase the efficiency. In addition, this system (battery, inverter, cabling, etc.) is already available in the market of HEVs [42]. In addition, automotive regulations demand costly shielded cabling (galvanic isolation) above 60V, so 48V systems keep the cost down. On the other hand, due to increase of the energy requirement, especially in pure electric mode, the parallel powertrain needs higher battery capacities and voltage. For this reason, batteries of 400 V with capacity higher than HEV were used. An inverter is used in conjunction with the battery pack template to ensure that the maximum discharge and charge power limits of the battery are not exceeded when it is connected to the electrical components. Table 7 shows more details of each parameter that was set in the DoE set up.

Table 7. Hybrid Powertrain Specifications.

Vehicle type	Parameter	Mild HEV	Parallel HEV
Electric Motor	Type [-]	IPM	
	Maximum power [kW]	3-25	10-60
	Weight [kg/kW] *	1.0	0.7
Battery Package	Type [-]	Lithium-Ion	
	Nominal voltage [V]	48	400
	Battery Capacity [Ah]	5-50	10-80
	Weight [kg/kWh] *	10.5	
	Initial SOC	0.64	

*Estimated as average of data provided by Sarlioglu et al. [2]

The three models (conventional, MHEV and P2-FHEV) contain a transmission to multiply the torque and speed from the propulsion system. The OEM transmission, which is a 6-gear ratio automatic transmission with gear ratios of: 3.8, 2.1, 1.3, 1.0, 0.7 and 0.6, was used in all the cases. The use of multi-gear transmission can effectively increase the remaining power of the engine. Consequently, the vehicle performance and fuel economy can be improved. The transmission control unit allows to change the gear depending on the vehicle speed. As the new normative WLTP [43] allows the vehicle manufacturer to choose the gear strategy, it was also optimized in this work. As reference parameter was taken the New European Driving Cycle (NEDC) fixed strategy [44] and was multiplied by a scaling factor (T_{mult}) that varies from 0.7 to 1.3. The variation of the operative condition for the conventional powertrain in the CDC engine map for the extreme values selected is depicted in the Appendix (Figure 27).

To evaluate the system and optimize the components, the simulations were carried out under the WLTC class 3b driving cycle, which is the homologation cycle currently in force for this type of vehicle [43]. It should be noted that this homologation is valid for conventional vehicles and non-plug in vehicles (MHEV and FHEV). The vehicle speed profile against time for the WLTC cycle is shown in Figure 8. This profile is entered into the driver model, which consists of a PID controller that determines the instantaneous power required to reach the speed demand and acts on the engine ECU giving the position of the accelerator in each instant.

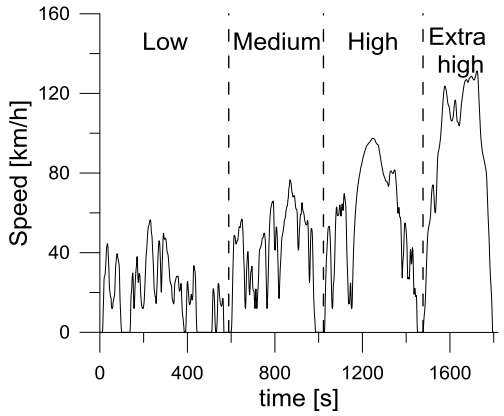

Figure 8 - Time-vehicle speed profiles of the WLTC cycle.

3. Results and discussion

The results are divided into two sections. The first one analyzes the DoE results for each powertrain in terms of performance, emissions and powertrain components. The second subsection is dedicated to compare the combustion modes and different powertrains in the optimal configuration achieved under WLTC driving cycle. All the results are compared with the results obtained with the OEM configuration (baseline case).

3.1. Optimization of the different hybrid concepts

3.1.1. Mild HEV

The mild hybrid powertrain was studied considering several EM and battery capacities. Additionally, the gear shift strategy was used as free parameter to optimize the zone used inside the ICE map. Figure 9 shows all the mild hybrid powertrain combinations tested with CDC (red points) and CDC-RCCI (blue points) engine maps that fulfill the condition of SOC_{end} equal to SOC_{target} and follow the WLTC driving cycle with a dispersion below 2%. In addition, the Pareto frontier line was inserted with the results obtained by the Kriging optimization, and the optimum point for each case was marked with square boxes. The graphs show a ‘‘boomerang’’ trend in which a great number of cases fall into the zone of low consumption (around 4.8 L/100km) and high NO_x emissions (around 0.65 g/km). Then, in the tail of this trend are cases with high fuel consumption but low or medium NO_x emission. This behavior is directly linked with the effect of the decrease of the shift coefficient T_{mult} (Figure 10a), which produce an increase of NO_x emissions and a reduction of the fuel consumption. The dual-mode CDC-RCCI combustion mode produces an important reduction in terms of NO_x emissions with almost all cases below the pure CDC engine map points. The combination of fuel and urea consumption (see Eq. 2) presented a slightly decrease (2%↓) for the CDC-RCCI, with higher difference in terms of NO_x emission (30%↓) than in fuel consumption (5%↑).

In addition, the battery capacity shows a trend (Figure 10b) in which a lower battery size improves the results in terms of total mass consumption (optimum around 5 Ah for both combustion concepts). This is mainly because the effect of increasing the vehicle weight, a parameter that affects directly to the fuel consumption. Below that point, the total mass consumption increases due to the lower power assist capabilities and more

charging periods. On the other hand, the electric motor size presents a flat trend in the range of size tested (2.5–25 kW) with the optimum being around 10 kW (see Figure 10b).

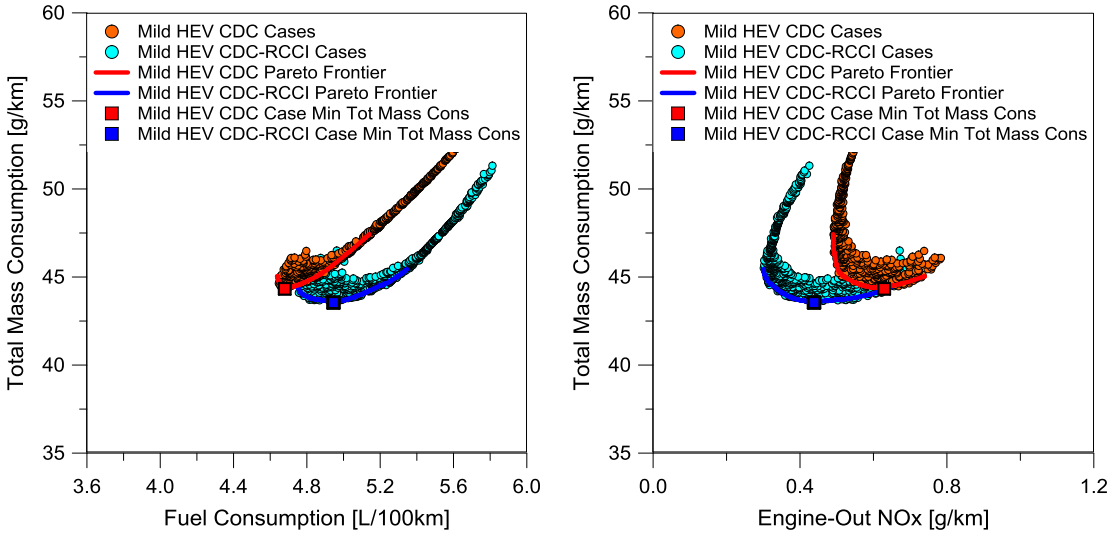

Figure 9 - Mild hybrid DOE results in terms of fuel consumption (a) and NO_x emission against total mass consumption.

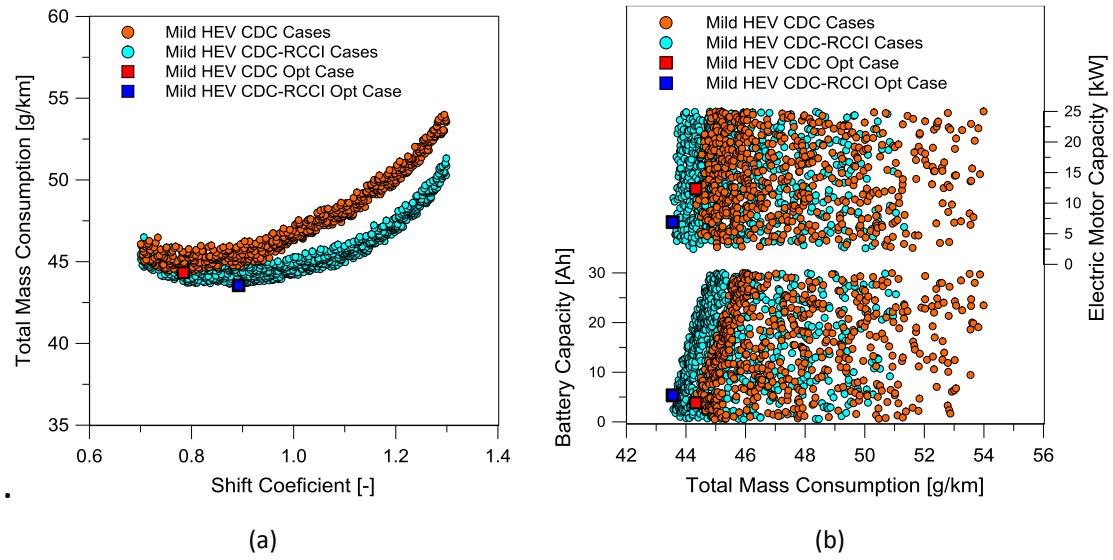

Figure 10 - Mild hybrid DOE results in terms of shift scaling coefficient (a) and battery and electric motor capacity (b) against total mass consumption.

A summary of the optimum cases was presented in the spider graph of Figure 11. As described above, CDC-RCCI improves the total mass consumption with an important reduction of NO_x emissions. The electric motor size and battery capacity was closer between the two combustion modes tested, suggesting that the main parameter to be changed when the engine maps is modified is the T_{mult}. This is expected because the RCCI patch in the CDC map allows to produce lower NO_x in the zone of 2500 RPM (T_{mult} = 0.90). Meanwhile, the CDC needs to maintain in the lower zone of engine speed to not produce high amount of NO_x (T_{mult} = 0.78). The total mass weight was closer to the OEM vehicle with a slight increase of 23 kg. This shows the advantage of this powertrain configuration, avoiding higher efforts of the manufactures to reduce the vehicle total mass.

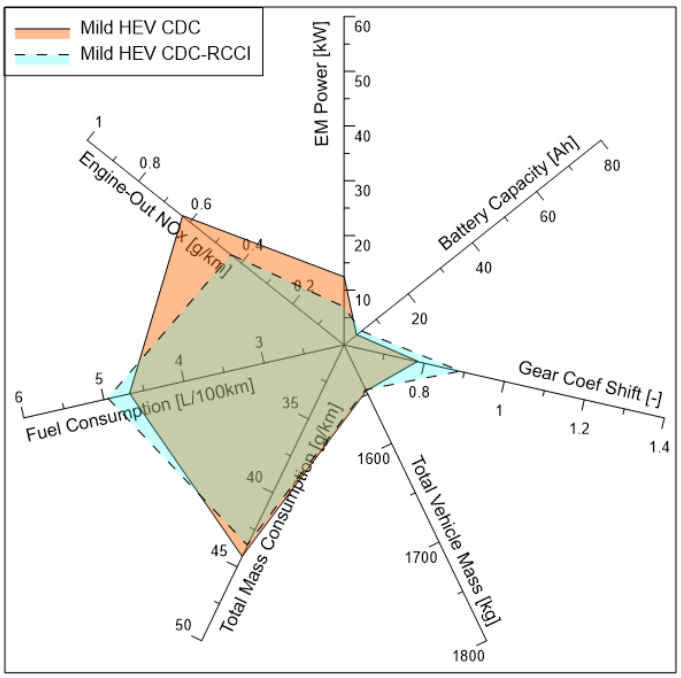

Figure 11- Main parameters for Mild hybrid optimum case for CDC and CDC-RCCI engine maps.

Figure 12 shows a comparison of the mild hybrid vehicle versus the baseline case (OEM Opel Vectra conventional diesel operation) with mild hybrid concepts in the WLTC driving cycle. The speed profile of the cycle (Figure 8) is depicted at the background of the figure. As it can be seen, the combination of mild HEV and CDC-RCCI technology offers the possibility to reduce the NO_x emissions without penalties in terms of fuel consumption in the fourth zones (low, medium, high and extra high). Moreover, for both hybrids concepts, the CDC-RCCI maps have only improvements in the total mass consumption at the end of the cycle (extra-high), where the urea consumption decreases with respect to the pure diesel map.

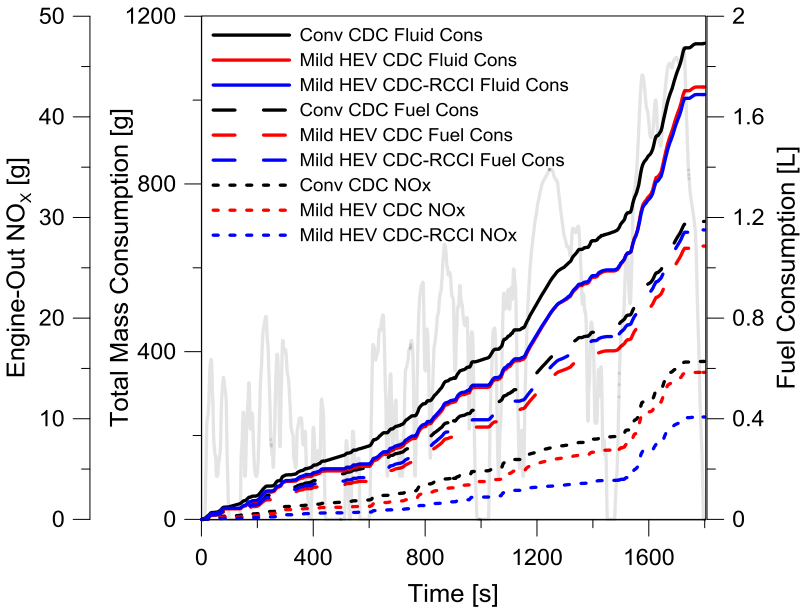

Figure 12 - Total mass consumption, fuel consumption and NO_x emissions along the WLTC driving cycle for conventional CDC, Mild hybrid CDC and Mild hybrid CDC-RCCI optimum cases.

3.1.2. Parallel HEV

A similar analysis was performed for the results obtained by the simulation code for P2-FHEV. The maximum speed to operate as pure electric mode was optimized in addition to the parameters included in the mild hybrid vehicle. It is important to note that higher EM and battery capacity can be tested due to the position of the electric motor between the ICE and the transmission. The results shown in Figure 13 have the same trend than that obtained with the MHEV. This is expected due to the similarities between the models and powertrain configuration. However, the P2-FHEV allows to achieve important reductions in terms of fuel consumption with respect to the OEM vehicle and MHEV. The T_{mult} (Figure 14a) is the main parameter that produce the trend in the total mass consumption against NO_x and fuel consumption due to the shift of the operative points in the engine map.

As can be seen in Figure 14b, the increase of the maximum vehicle speed for the pure electric mode decreases the total mass consumption. In spite of that the optimum points for both combustion modes were found around 100 km/h, above this vehicle velocity the trend is flat without great increments. This could be associated to that the SOC_{charge} limit is the parameter that restricts the pure electric mode instead of the vehicle speed.

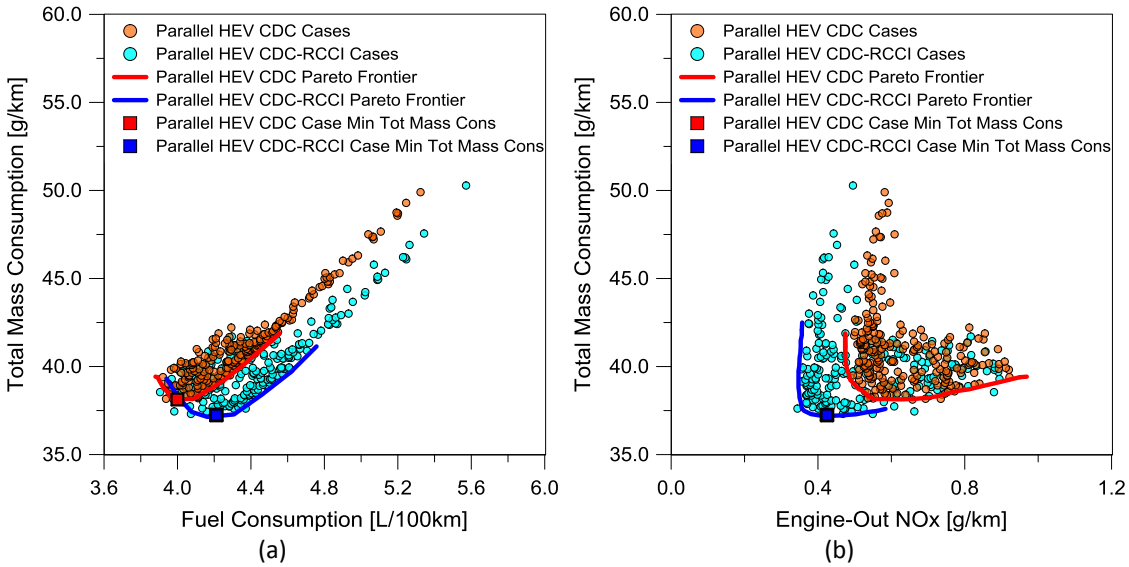

Figure 13 – Parallel hybrid DOE results in terms of fuel consumption (a) and NOx emission (b) against total mass consumption.

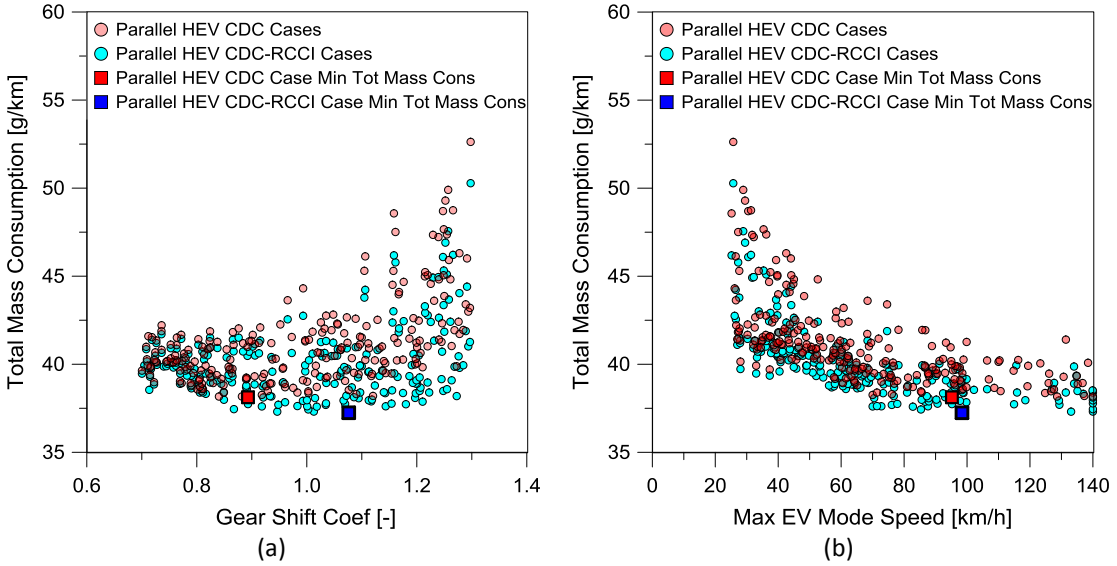

Figure 14 – Parallel hybrid DOE results in terms of shift scaling coefficient (a) and vehicle speed limit to pure electric vehicle mode (b) against total mass consumption.

The electric motor and battery size present a flat trend in the range of size tested, 20-60 kW and 10-80 Ah respectively. Also, there were small differences between both combustion modes tested. For the sake of brevity, the graphs were not included in the manuscript. However, the final results for the optimum case are presented in the spider graph of Figure 15. In terms of battery capacity, the best cases were seen around 50 Ah, that represents the zone of high battery capacity. On the other hand, for the electric motor capacity the optimum was reached in the zone of medium EM size (30 kW for CDC-RCCI and 40 kW for CDC).

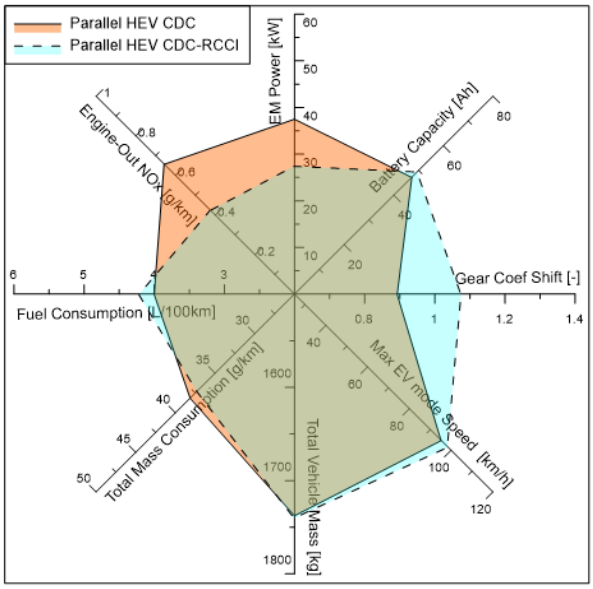

Figure 15- Main parameters for Parallel hybrid optimum case for CDC and CDC-RCCI engine maps.

Figure 16 shows the instantaneous fluid consumptions and NO_x emissions for the parallel HEVs and OEM vehicle along the WLTC. Among the high reduction in total mass and fuel consumption with respect to the conventional powertrain, the high advantage of this hybrid technology is the shift of the emissions produced from the low and medium to the high and extra-high zones. This could strongly contribute to reduce the local air pollution in the cities, specially avoiding the emission of NO_x and soot. The P2-FHEV in the optimum case, for both engine maps (CDC and CDC-RCCI), provide pure electric operation in the 60% of the cycle due to the high battery capacity. The total NO_x emissions were reduced in the CDC-RCCI map. However, for CDC engine maps the difference between hybrid and conventional powertrain was minimum. This behavior is because in the extra-high zone for P2-FHEV, the ICE needs to give power to both the wheels and the EM to charge the battery operating in the highest power zone.

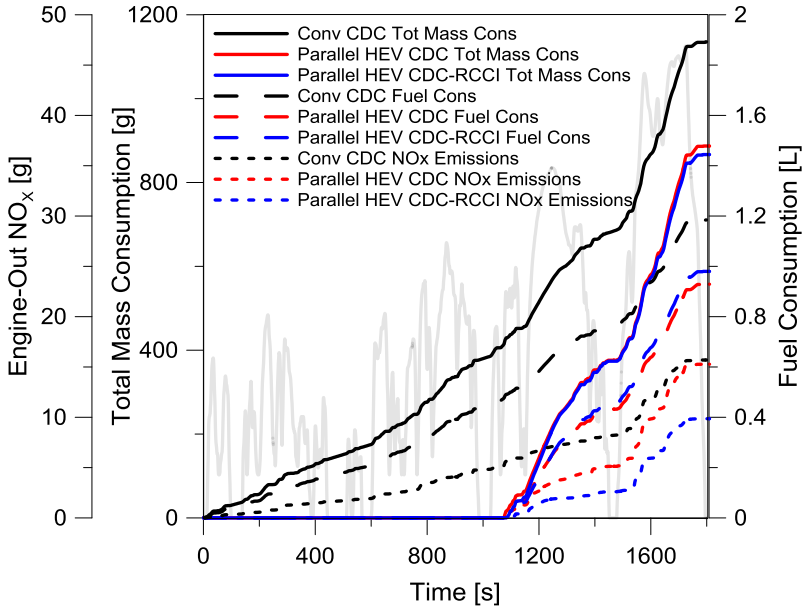

Figure 16 - Total mass consumption, fuel consumption and NO_x emissions along the WLTC driving cycle for conventional CDC, Parallel hybrid CDC and Parallel hybrid CDC-RCCI optimum cases.

3.2. Comparison of the optimized concepts

This section aims to give a global vision of the results found in the previous sections. After the optimization of each powertrain and selection of the optimal case to perform the WLTC cycle, the advantages of the proposed models can be analyzed. Figure 17a shows that the parallel full hybrid vehicle allows the highest reduction in the total fluid mass consumption (fuel + urea), around 22% with respect to the OEM vehicle. On the other hand, the MEHV shows intermediate gains with a reduction of 9%. Focusing on the combustion modes, it is possible to see in the graph that with the use of the RCCI mode inside the map of CDC, a reduction of 3% in the fluid mass consumption could be obtained with respect to the same powertrain technology but in pure CDC mode.

However, the total gain in each vehicle concept do not come from the same point. In the case of CDC, the major gain comes from the reduction in the fuel consumption, as shown in Figure 17b. By contrast, in the dual-mode CDC-RCCI, the reason of the reduction is twofold, great part of the reduction comes from the lower fuel consumption and another part comes from the lower urea consumption (Figure 18a). The SCR equipment allows to reduce the NOx emission up to the Euro 6 level (0.08 g/km) as can be seen in Figure 18b. Moreover, the dual-mode CDC-RCCI reduces the urea mass consumption from 5 g/km in pure CDC to 3 g/km. Another important fact shown in Figure 12 and Figure 16 is the lower NO_x emissions in urban areas for the parallel model. This show the potential of the studied technology to reduce the local air pollution that is so much sought by government agencies.

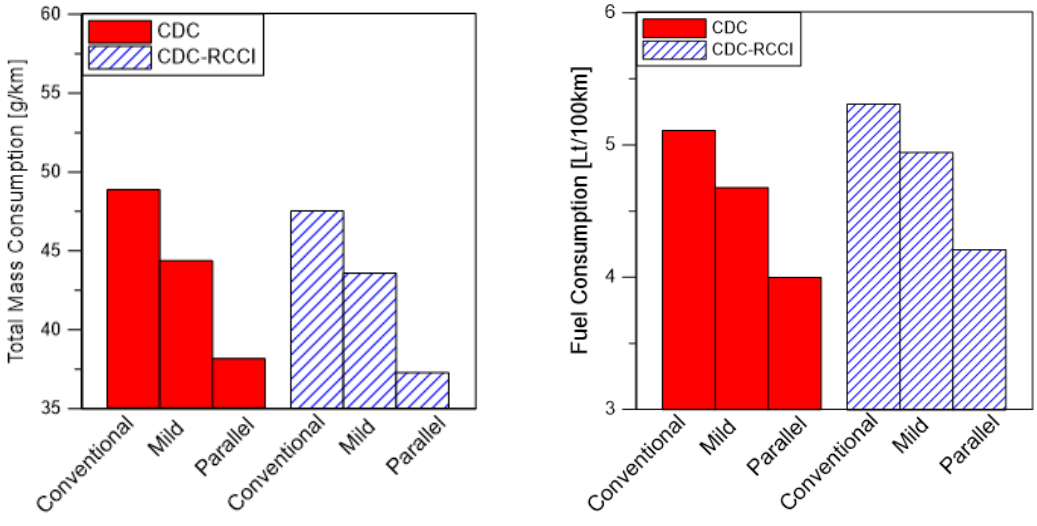

Figure 17 – Total mass consumption [g/km] (a) and fuel consumption [L/100km] (b) for conventional, MHEV and P2-FHEV with CDC and CDC-RCCI engine maps in the WLTC driving cycle.

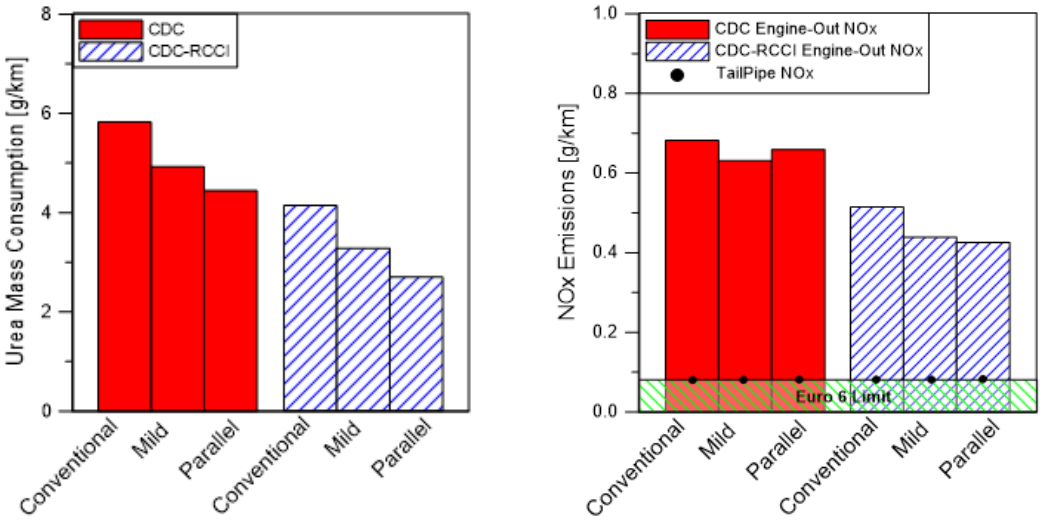

(a) (b)

Figure 18 – Urea mass consumption in the SCR aftertreatment equipment [g/km] (a) and Engine-out NOx emissions [g/km] and Tail-Pipe NOx emission after the SCR-Urea aftertreatment equipment for conventional, MHEV and P2-FHEV with CDC and CDC-RCCI engine maps in the WLTC driving cycle.

Another advantage of the proposed powertrain models is the increase of the power of the vehicles over the whole speed range of the engine, as shown in Figure 19. For the case FHEV-P2, the maximum power is reached at 140 kW, about 35 kW more than the conventional vehicle. It is important to note that several authors [27,45] affirm that a considerable improvement in the fuel consumption can be carried out with the addition of the downsizing trend in ICE. Therefore, with an engine of lower capacity and designed to operate in these advanced powertrains, it could be reached greater benefits than the results presented in this work. For example, re-calibration of the engine maps in the RCCI and CDC modes to achieve lower emissions when operated with EM assistance.

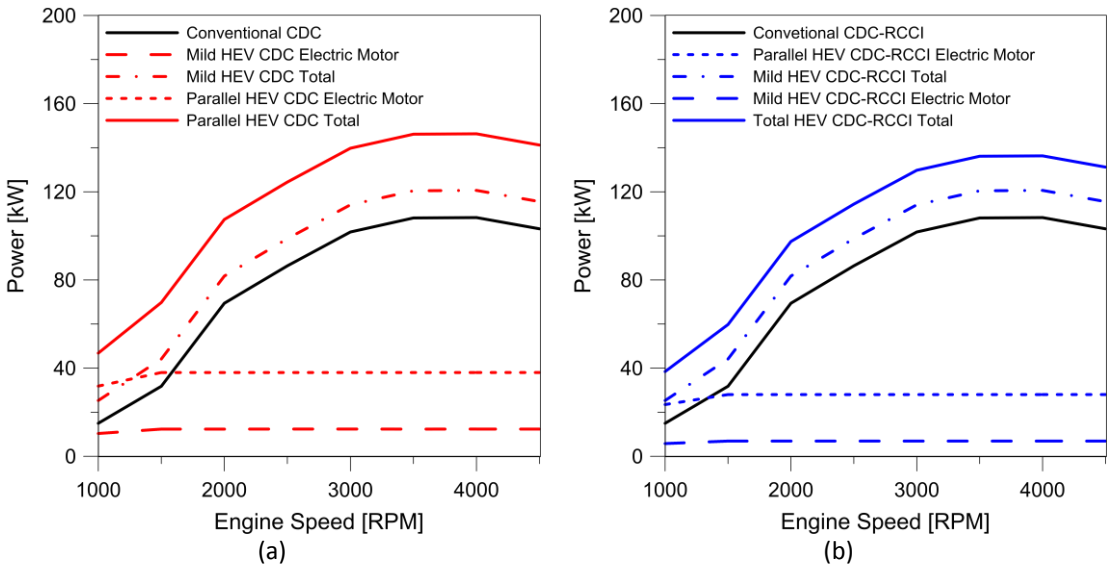

(a) (b)

Figure 19 – Vehicle power in the operative range of the ICE for CDC maps (a) CDC-RCCI maps for MHEV and P2-FHEV optimum cases and comparison with conventional powertrain.

In addition to the potential of reducing the total fuel consumption and local air pollution, the hybrid technology also contributes to reduce total CO_2 (Figure 20a), which is one of the main concerns of the future emissions legislations to reduce the global

warming. P2-FHEV reduces the CO_2 emissions by 35% compared to CDC, while MHEV is capable to promote a 16% reduction. The difference between combustion modes, CDC and CDC-RCCI, is minimum whenever the powertrain proposed. However, as seen in Figure 20b, adding a RCCI zone in the CDC map allows an important reduction of soot emissions (around 40%). The results also show that introducing both technologies, a Euro 4 OEM calibration could be worth to operate fulfilling the Euro 6 soot emissions. As was expected considering the engine maps depicted in Figure 24 and Figure 25 of the Appendix, HC and CO emissions have a large increment in the CDC-RCCI combustion mode (Figure 21).

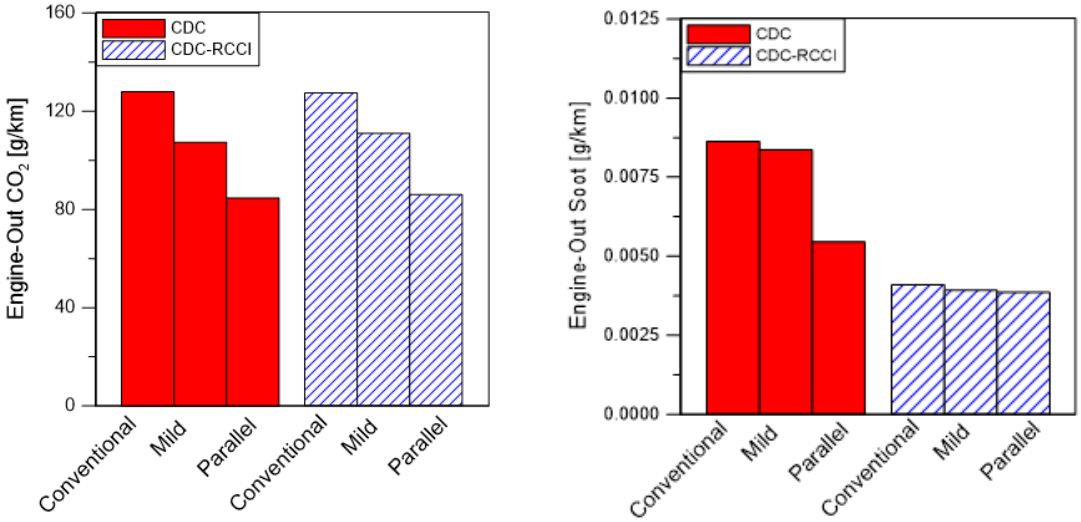

Figure 20 – CO_2 emissions [g/km] (a) and Soot emissions [g/km] (b) for conventional, MHEV and P2-FHEV with CDC and CDC-RCCI engine maps in the WLTC driving cycle.

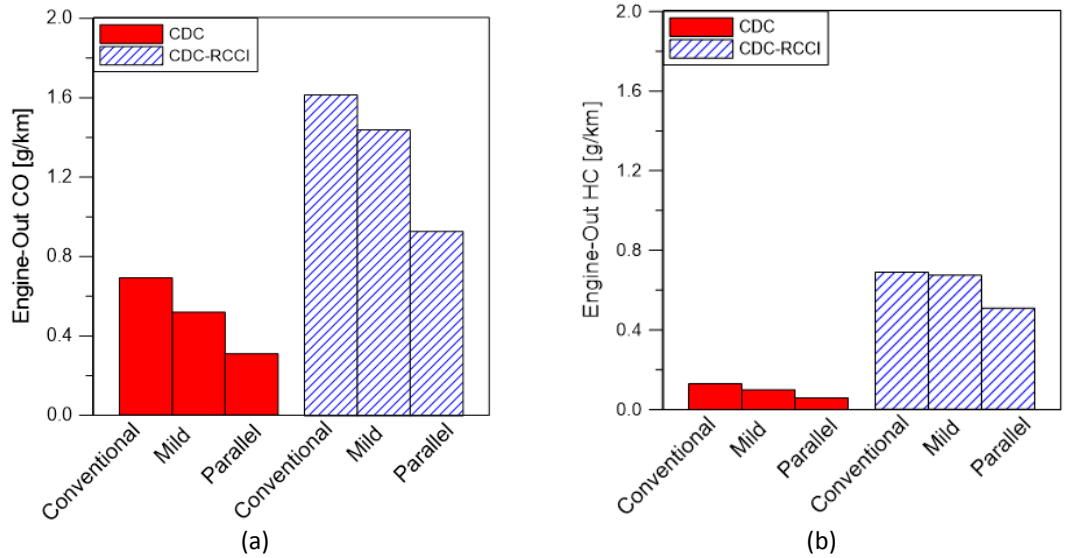

Figure 21 – CO emissions [g/km] (a) and HC emissions [g/km] (b) for conventional, MHEV and P2-FHEV with CDC and CDC-RCCI engine maps in the WLTC driving cycle.

Finally, Figure 22 shows the gasoline fraction used in the CDC-RCCI combustion mode for each powertrain simulated. Figure 22a shows the gasoline mass percentage against the total mass for all the simulated cases and Figure 22b shows the values for the optimum points for conventional, MHEV and P2-FHEV. From Figure 22a, it is possible

to see that parallel powertrain operates in a lower zone (around 38 g/km) in terms of total mass consumption for all cases than the other models (around 47 g/km) despite the gasoline fraction. However, it can be seen a slight reducing trend of the total mass consumption as the gasoline fraction is increased. The optimum case of the MHEV model presents higher percentage of gasoline than the parallel and conventional powertrains. This behavior can be attributed to the effect of better distribution between ICE-EM power for the MHEV than in P2-FHEV and not necessity of large recharging periods that induce the engine to operate at high power loads. However, due to the small zone of RCCI in the CDC map, it was not possible to reach 40% in any case of study.

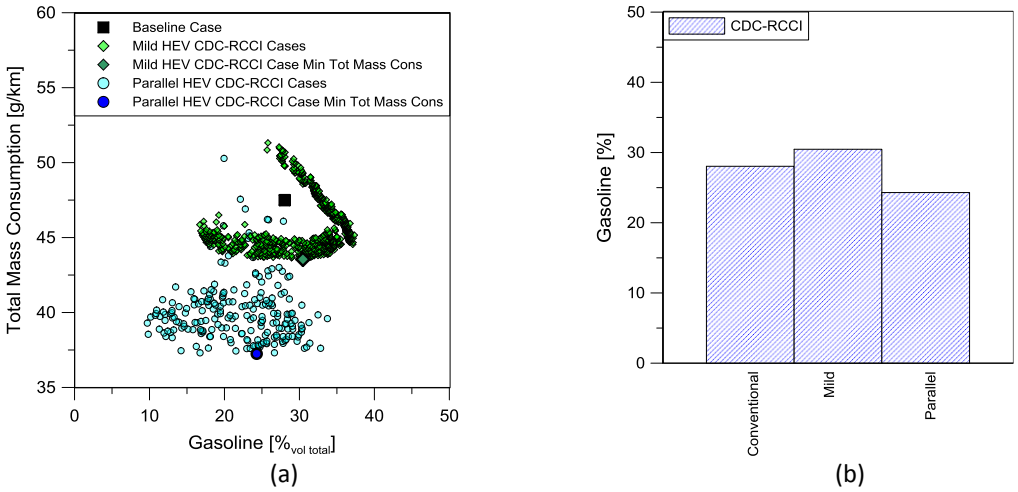

Figure 22 – Gasoline proportion [%] in total fuel volume used in the CDC-RCCI combustion modes by hybrid powertrains for all cases (a) and the optimum case (b) in the WLTC driving cycle.

4. Conclusions

This work investigated the performance of two hybrid powertrains adapted to a D-segment conventional powertrain vehicle equipped with a diesel 1.9L GM engine. Mild and P2 full hybrid architectures were simulated with the experimental maps for CDC and CDC-RCCI combustion modes previously obtained as inputs. A multi-objective Pareto optimization process was carried out to determine the best configuration in terms of electric motor and battery size, among the transmission shift strategy for a WLTC driving cycle. From this study, it was found that:

- P2-FHEV provides the major gains in terms of fuel consumption for CDC and CDC-RCCI combustion modes. The best configuration was found with high battery capacity (50 Ah), medium EM size (around 35 kW) and 100 km/h as limit for the pure electric speed mode.
- MHEV allows intermediate fuel consumption reduction when compared to conventional powertrain and P2-FHEV. The optimal solution for the powertrain elements was found with low battery capacity (5Ah) and EM around 10% of the ICE maximum power.
- The main parameter to be optimized between the two combustion modes is the gear shifting strategy. The CDC show the best configuration, with a shifting coefficient with respect to the NEDC fix strategy near 0.8, and CDC-RCCI near 1.0.

The results of instantaneous fuel consumption show the advantages of hybridization in urban traffic. This is due to the energy gain of the regenerative braking and the lower power demand of the combustion engine under these conditions. The ICE returns this energy in more efficient conditions such as the high and extra high zone, resulting in greater total energy savings. For the parallel hybrid vehicle, the pure electric mode allows to not start the engine until the high phase of the driving cycle. This point, together with the reduction of fuel consumption and CO_2 emission, evidences the potential of this technology to reduce local and global air pollution.

Finally, the use of RCCI zone inside the conventional diesel combustion mode allows a reduction of the total mass consumption (fuel plus urea) and NOx emission at the tailpipe. Cases up to 40% of gasoline in the total fuel volume were allowed with the small RCCI zone used in this work. However, the optimum case for the three powertrains were found around 28%.

Acknowledgments

The authors want to express their gratitude to General Motors Global Research & Development for providing the engine used to acquire the experimental data used in this investigation. The authors acknowledge FEDER and Spanish Ministerio de Economía y Competitividad for partially supporting this research through TRANCO project (TRA2017-87694-R). The authors also acknowledge the Universitat Politècnica de València for partially supporting this research through Convocatoria de ayudas a Primeros Proyectos de Investigación (PAID-06-18).

References

[1] Huang Y, Wang H, Khajepour A, Li B, Ji J, Zhao K, et al. A review of power management strategies and component sizing methods for hybrid vehicles. Renew Sustain Energy Rev 2018;96:132–44. doi:10.1016/j.rser.2018.07.020.

[2] Sarlioglu B, Morris CT, Han D, Li S. Benchmarking of electric and hybrid vehicle electric machines, power electronics, and batteries. 2015 Intl Aegean Conf. Electr. Mach. Power Electron. (ACEMP), 2015 Intl Conf. Optim. Electr. Electron. Equip. 2015 Intl Symp. Adv. Electromechanical Motion Syst., IEEE; 2015, p. 519–26. doi:10.1109/OPTIM.2015.7426993.

[3] Cubito C, Millo F, Boccardo G, Di Pierro G, Ciuffo B, Fontaras G, et al. Impact of different driving cycles and operating conditions on CO2emissions and energy management strategies of a Euro-6 hybrid electric vehicle. Energies 2017;10. doi:10.3390/en10101590.

[4] He H, Guo X. Multi-objective optimization research on the start condition for a parallel hybrid electric vehicle. Appl Energy 2018;227:294–303. doi:10.1016/j.apenergy.2017.07.082.

[5] Piechottka H, Küçükay F, Kercher F, Bargende M. Optimal Powertrain Design through a Virtual Development Process. World Electr Veh J 2018;9:11. doi:10.3390/wevj9010011.

[6] Huang Y, Surawski NC, Organ B, Zhou JL, Tang OHH, Chan EFC. Fuel consumption and emissions performance under real driving: Comparison between hybrid and conventional vehicles. Sci Total Environ 2019;659:275–82. doi:10.1016/j.scitotenv.2018.12.349.

[7] Solouk A, Shakiba-herfeh M, Shahbakhti M. Analysis and Control of a Torque Blended Hybrid Electric Powertrain with a Multi-Mode LTC-SI Engine. SAE Int J Altern Powertrains 2017;6:2017-01-1153. doi:10.4271/2017-01-1153.

[8] Liu Z, Ivanco A, Onori S. Aging characterization and modeling of nickel-manganese-cobalt lithium-ion batteries for 48V mild hybrid electric vehicle applications. J Energy Storage 2019;21:519–27. doi:10.1016/j.est.2018.11.016.

[9] Gan S, Chrenko D, Kéromnès A, Le Moyne L. Development of a Multi-Architecture and Multi-Application Hybrid Vehicle Design and Management Tool. Energies 2018;11:3185. doi:10.3390/en11113185.

[10] Karaoğlan MU, Kuralay NS, Colpan CO. The effect of gear ratıos on the exhaust emıssıons and fuel consumptıon of a parallel hybrid vehicle powertrain. J Clean Prod 2019;210:1033–41. doi:10.1016/j.jclepro.2018.11.065.

[11] Karaoğlan MU, Kuralay NS, Colpan CO. The effect of gear ratıos on the exhaust emıssıons and fuel consumptıon of a parallel hybrid vehicle powertrain. J Clean Prod 2018;210:1033–41. doi:10.1016/j.jclepro.2018.11.065.

[12] Hu D, Hu L, Yan Y. Optimization methodology for control strategy of parallel hybrid electric vehicle based on chaos prediction. AIP Adv 2018;8:115305. doi:10.1063/1.5055644.

[13] Zhou W, Yang L, Cai Y, Ying T. Dynamic programming for New Energy Vehicles based on their work modes part I: Electric Vehicles and Hybrid Electric Vehicles. J Power Sources 2018;406:151–66. doi:10.1016/j.jpowsour.2018.10.047.

[14] Arthanari T, S SK. Simulation-Driven Approach to Design & amp; Evaluate Vehicle Thermal Management. WCX World Congr. Exp., 2018. doi:10.4271/2018-01-1183.

[15] Benajes J, García A, Monsalve-Serrano J, Lago Sari R. Fuel consumption and engine-out emissions estimations of a light-duty engine running in dual-mode RCCI/CDC with different fuels and driving cycles. Energy 2018;157:19–30. doi:10.1016/j.energy.2018.05.144.

[16] Fayad MA, Fernández-Rodríguez D, Herreros JM, Lapuerta M, Tsolakis A. Interactions between aftertreatment systems architecture and combustion of oxygenated fuels for improved low temperature catalysts activity. Fuel 2018;229:189–97. doi:10.1016/j.fuel.2018.05.002.

[17] García A, Monsalve-Serrano J, Rückert Roso V, Santos Martins ME. Evaluating the emissions and performance of two dual-mode RCCI combustion strategies under the World Harmonized Vehicle Cycle (WHVC). Energy Convers Manag 2017;149:263–74. doi:10.1016/j.enconman.2017.07.034.

[18] Benajes J, Tormos B, Garcia A, Monsalve-Serrano J. Impact of Spark Assistance and Multiple Injections on Gasoline PPC Light Load 2014. doi:https://doi.org/10.4271/2014-01-2669.

[19] Kokjohn SL, Hanson RM, Splitter DA, Reitz RD. Experiments and Modeling of Dual-Fuel HCCI and PCCI Combustion Using In-Cylinder Fuel Blending. SAE Int J Engines 2009;2:2009-01-2647. doi:10.4271/2009-01-2647.

[20] Manente V, Tunestal P, Johansson B, Cannella WJ. Effects of Ethanol and Different Type of Gasoline Fuels on Partially Premixed Combustion from Low to High Load 2010. doi:10.4271/2010-01-0871.

[21] Benajes J, García A, Monsalve-Serrano J, Balloul I, Pradel G. Evaluating the reactivity controlled compression ignition operating range limits in a high-compression ratio medium-duty diesel engine fueled with biodiesel and ethanol. Int J Engine Res 2017;18:66–80. doi:10.1177/1468087416678500.

[22] Benajes J, García A, Monsalve-Serrano J, Sari R. Potential of RCCI Series Hybrid Vehicle Architecture to Meet the Future CO2 Targets with Low Engine-Out Emissions. Appl Sci 2018;8:1472. doi:10.3390/app8091472.

[23] Benajes J, García A, Monsalve-Serrano J, Boronat V. Dual-Fuel Combustion for Future Clean and Efficient Compression Ignition Engines. Appl Sci 2016;7:36. doi:10.3390/app7010036.

[24] Taymaz I, Benli M. Emissions and fuel economy for a hybrid vehicle. Fuel 2014;115:812–7. doi:10.1016/j.fuel.2013.04.045.

[25] Hooftman N, Messagie M, Van Mierlo J, Coosemans T. A review of the European passenger car

regulations – Real driving emissions vs local air quality. Renew Sustain Energy Rev 2018;86:1–21. doi:10.1016/j.rser.2018.01.012.

[26] Benajes J, García A, Monsalve-Serrano J, Villalta D. Exploring the limits of the reactivity controlled compression ignition combustion concept in a light-duty diesel engine and the influence of the direct-injected fuel properties. Energy Convers Manag 2018;157:277–87. doi:10.1016/j.enconman.2017.12.028.

[27] Morra E, Spessa E, Ciaravino C, Vassallo A. Analysis of Various Operating Strategies for a Parallel-Hybrid Diesel Powertrain with a Belt Alternator Starter. SAE Int J Altern Powertrains 2012;1:2012-01-1008. doi:10.4271/2012-01-1008.

[28] Capata R. Urban and Extra-Urban Hybrid Vehicles: A Technological Review. Energies 2018;11:2924. doi:10.3390/en11112924.

[29] Ali AM. Towards Optimal Power Management of Hybrid Electric Vehicles in Real-Time: A Review on Methods, Challenges, and State-Of-The-Art Solutions. Energies 2018;11:476. doi:10.3390/en11030476.

[30] Wirasingha SG, Emadi A. Classification and review of control strategies for plug-in hybrid electric vehicles. IEEE Trans Veh Technol 2011;60:111–22. doi:10.1109/TVT.2010.2090178.

[31] Wang R, Yu W, Meng X. Performance investigation and energy optimization of a thermoelectric generator for a mild hybrid vehicle. Energy 2018;162:1016–28. doi:10.1016/j.energy.2018.08.103.

[32] Lee S, Lee B, McDonald J, Sanchez LJ, Nam E. Modeling and Validation of Power-Split and P2 Parallel Hybrid Electric Vehicles. SAE 2013 World Congr. Exhib., 2013. doi:10.4271/2013-01-1470.

[33] García A, Monsalve-Serrano J, Sari R, Dimitrakopoulos N, Tunér M, Tunestål P. Performance and emissions of a series hybrid vehicle powered by a gasoline partially premixed combustion engine. Appl Therm Eng 2019;150:564–75. doi:10.1016/j.applthermaleng.2019.01.035.

[34] OLIVER MA, WEBSTER R. Kriging: a method of interpolation for geographical information systems. Int J Geogr Inf Syst 1990;4:313–32. doi:10.1080/02693799008941549.

[35] Luján JM, Bermúdez V, Dolz V, Monsalve-Serrano J. An assessment of the real-world driving gaseous emissions from a Euro 6 light-duty diesel vehicle using a portable emissions measurement system (PEMS). Atmos Environ 2018;174:112–21. doi:10.1016/j.atmosenv.2017.11.056.

[36] Johnson T V. Diesel Emissions in Review 2011. doi:https://doi.org/10.4271/2011-01-0304.

[37] V J, D D. The Kinetic Energy Storage as an Energy Buffer for Electric Vehicles. Adv Automob Eng 2017;06. doi:10.4172/2167-7670.1000165.

[38] Bae SH, Park JW. A study on optimal operation strategy for mild hybrid electric vehicle based on hybrid energy storage system. J Electr Eng Technol 2018;13:631–6.

[39] Bao R, Avila V, Baxter J. Effect of 48 V Mild Hybrid System Layout on Powertrain System Efficiency and Its Potential of Fuel Economy Improvement. WCX™ 17 SAE World Congr. Exp., SAE International; 2017. doi:https://doi.org/10.4271/2017-01-1175.

[40] Vallur AR, Khairate Y, Awate C. Prescriptive Modeling, Simulation and Performance Analysis of Mild Hybrid Vehicle and Component Optimization. Symp. Int. Automot. Technol. 2015, SAE International; 2015. doi:https://doi.org/10.4271/2015-26-0010.

[41] Nikolian A, Firouz Y, Gopalakrishnan R, Timmermans JM, Omar N, van den Bossche P, et al. Lithium ion batteries-development of advanced electrical equivalent circuit models for nickel manganese cobalt lithium-ion. Energies 2016;9:360. doi:10.3390/en9050360.

[42] Yoon K, Hong J, Shim J. A Study on Front End Auxiliary Drive(FEAD) System of 48V Mild Hybrid

Engine. WCX World Congr. Exp., SAE International; 2018. doi:https://doi.org/10.4271/2018-01-0414.

[43] Nations U. Global technical regulation No. 15 on Worldwide harmonized Light vehicles Test Procedure (WLTP). 2015.

[44] EUROPEAN COMMISSION. Regulated emissions of a Euro 5 passenger car measured over different driving cycles 2010:23.

[45] Shen C, Shan P, Gao T. A Comprehensive Overview of Hybrid Electric Vehicles. Int J Veh Technol 2011;2011:1–7. doi:10.1155/2011/571683.

Abbreviations

BAS	Belted Alternator Starter	m_{fuel}	Fuel mass consumption
BMS	Battery management system	MHEV	Mild hybrid electric vehicle
CDC	Conventional diesel combustion	$m_{totmasscons}$	Total mass consumption
Charge $_T$	Torque assigned to charge the battery	m_{urea}	Urea mass conumption
DI	Direct Injection	NEDC	New
DoE	Design of Experiments	NIMH	New European Driving Cycle
ECU	Engine control unit	NOxEU6	Nitrogen oxide limit for Euro 6 legislation
EGR	Exhaust gas recirculation	OEM	Oroiginal equipment manufacturer
EM	Electric motor	P2-FHEV	Parallel full hybrid electric vehicle
EMS	Energy managment system	PFI	Port fuel injection
EV	Electric vehicle	PHEV	Plug in electric vehicle
FSN	Filter smoke number	PPC	Partially premixed combustion
GM	General Motors	RBC	Rule base control
HCCI	Homogeneous charge compression ignition	RCCI	Reactivity controlled compression ignition
HEV	Hybrid electric vehicle	RPM	Revolution per minute
IM	Induction motor	SOC	State of the charge of the battery
IPM	Interior permanent magnet	SPM	Permanent magnet machine
LI-Ion	Litium Ion batteries	T_{mult}	Transmission gear shift multiplier
LTC	Low temperature combustion	V	Vehicle speed
WLTC	Worldwide Harmonized Light Vehicles Cycle		

Appendix

Engine maps for CO_2, HC, CO and Soot in CDC and CDC-RCCI mode. For this last case the dual fuel zone is marked with dashed lines.

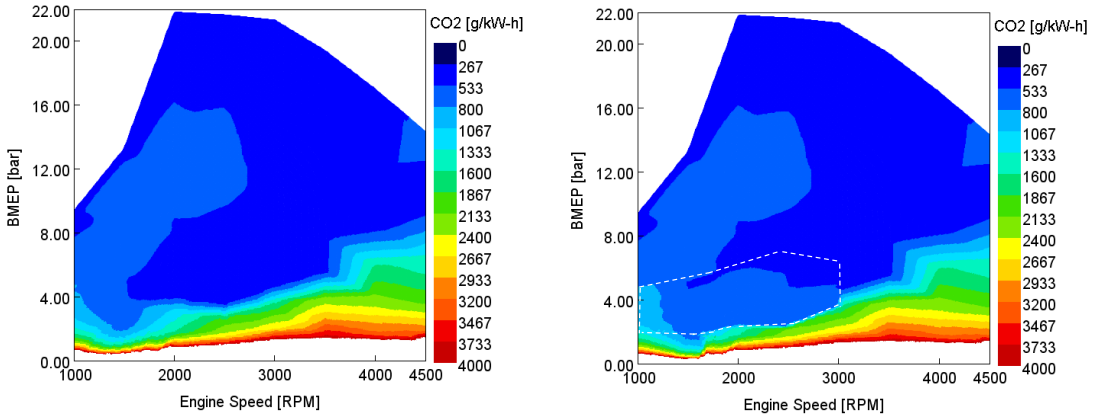

Figure 23. CO_2 emission (g/kWh) for pure diesel (a) and the dual-mode CDC-RCCI concept (b).

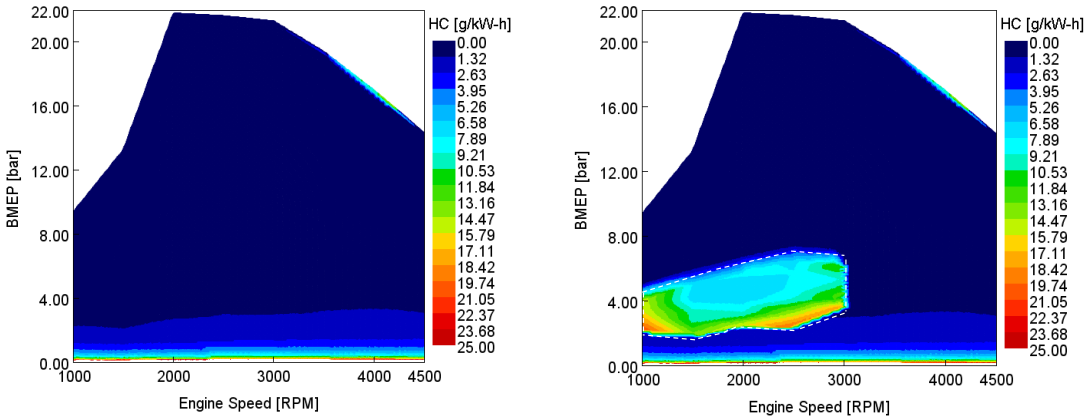

Figure 24. HC emission (g/kWh) for pure diesel (a) and the dual-mode CDC-RCCI concept (b).

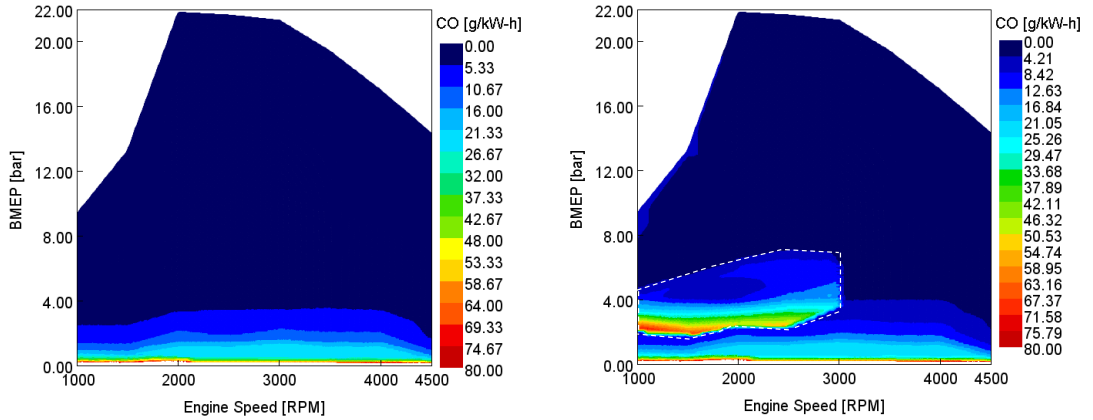

Figure 25. CO emission (g/kWh) for pure diesel (a) and the dual-mode CDC-RCCI concept (b).

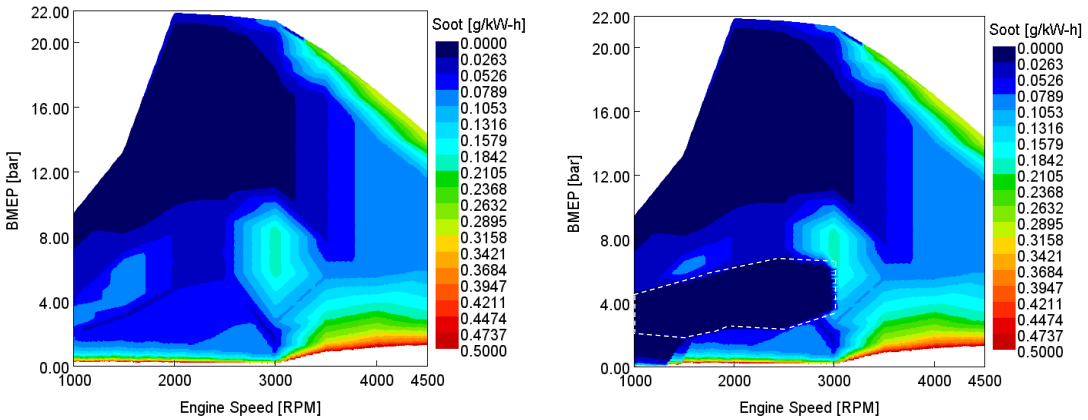

(a) (b)

Figure 26. Soot emission (g/kWh) for pure diesel (a) and the dual-mode CDC-RCCI concept (b).

Operative conditions for conventional powertrain with traction shift multiplier in the extreme case of the range selected (0.7 and 1.3). This coefficient multiplies the speed limit for each gear change of the strategy used for NEDC driving cycle. As in the WLTC is a free parameter, it needs to be optimized for each configuration.

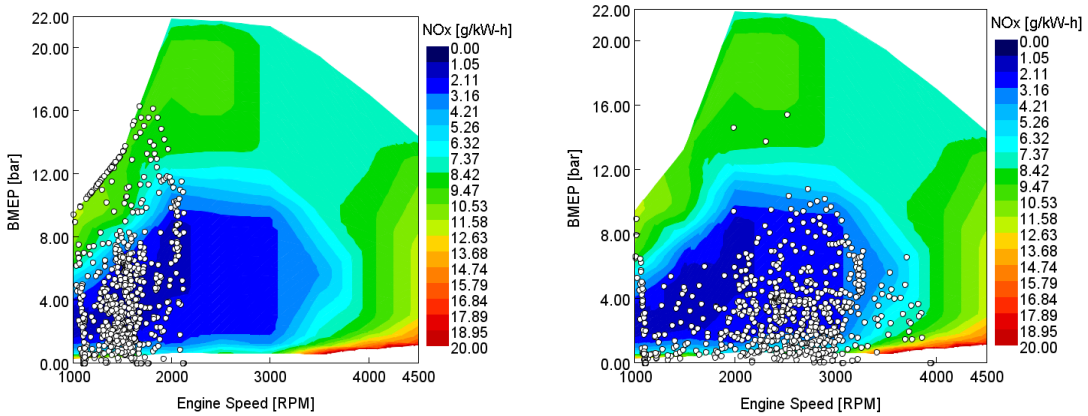

(a) (b)

Figure 27. Operative condition for conventional powertrain with traction shif multiplier set at: 0.7 (a) and 1.3 (b).